Bioinspired 4D Printed Tubular/Helicoidal Shape Changing Metacomposites for Programmable Structural Morphing

A. Le Duigou, M. Grabow, F. Scarpa, J. Deschamps, C. Combescure, K. Labstie, Justin Dirrenberger, M. Castro, U. Lafont

Bioinspired 4D Printed Tubular/Helicoidal Shape Changing Metacomposites for Programmable Structural Morphing

A. Le Duigou, M. Grabow, F. Scarpa, J. Deschamps, C. Combescure, K. Labstie, J. Dirrenberger, M. Castro, and U. Lafont*

Biological structures combine passive shape-changing with force generation through intricate composite architectures. Natural fibers, with their tubular-like structures and responsive components, have inspired the design of pneumatic tubular soft composite actuators. However, no development of passive structural actuation is available despite the recent rise of 4D printing. In this study, a biomimicry approach is proposed with inspiration from natural fiber architecture to create a novel concept of thermally active 4D printed tubular metacomposites. These metacomposites exhibit high mechanical performance and 3D-to-3D shape-changing ability triggered by changes in temperature. A rotative printer is proposed for winding a continuous carbon fibers reinforced PolyAmide 6.I composite on a PolyAmide 6.6 polymer mandrel in a similar manner to the structure of cellulose microfibrils within the polysaccharide matrix of natural fiber cell-walls. The resulting 4D printed tubular metacomposites exhibit programmable rotation and torque in response to thermal variations thanks to the control of their mesostructure and the overall geometry. Energy density values representing a trade-off between the rotation and the torque are comparable to shape memory alloys when normalized by stiffness. Finally, a proof of concept for an autonomous solar tracker is presented, showcasing its potential for designing autonomous assemblies for structure morphing.

1. Introduction

In the plant kingdom certain seed spreading and germination processes involve autonomous, complex morphing abilities with various morphological transitions. These processes integrate moisture sensing and actuation within a single biological structure, such as natural fiber cell walls.[1] The latter have no muscles and rely on differential growth or expansion and material distribution to achieve complex and sequential shape changes.[2] A large taxonomy of shape-changes can be observed in plants: bending/curvature, folding, helixing, twisting, contraction/expansion, or combinations of those. In addition to shape-changing, natural fiber structures can demonstrate seemingly contradictory properties by combining stiffness with shape-changing for passive structural morphing.[3] Natural fibers consist in stiff cellulose winded in helicoidal shapes and embedded in a compliant polysaccharide matrix within a tubular-like architecture.[4] These geometries are particularly of interest[5] when compared to planar architectures, as they allow to reach over 50% more work for a similar volume.[6]

Biomimicry is a critical toll for developing new paradigmatic materials, particularly for soft robotics or adaptive architectural systems, where extreme environments pose limiting factors.[7,8] In addition, the remarkable multifunctionality of biological structures

A. Le Duigou, M. Grabow, J. Deschamps, C. Combescure, M. Castro
IRDL UMR CNRS 6027, Bionics group, Centre de recherche C Huygens, Université de Bretagne Sud
Lorient, France
E-mail: antoine.le-duigou@univ-ubs.fr

A. Le Duigou, J. Dirrenberger
Institut Universitaire de France (IUF)
Paris, France

F. Scarpa
Aerospace Engineering
Bristol Composites Institute
School of Civil
Aerospace and Design Engineering (CADE)
University of Bristol
Bristol BS8 1TR, UK

C. Combescure
Saint-Cyr Coetquidan Military Academy
CReC Saint-Cyr
Guer 56380, France

K. Labstie
IRT Saint-Exupéry
Toulouse 31405, France

J. Dirrenberger
Laboratoire PIMM
Arts et Métiers-ParisTech
CNAM, CNRS
Paris 75013, France

U. Lafont
European Space Research and Technology Centre
European Space Agency
Keplerlaan 1, Noordwijk 2201 AZ, The Netherlands

The ORCID identification number(s) for the author(s) of this article can be found under https://doi.org/10.1002/admt.202400237

DOI: 10.1002/admt.202400237

is achieved by combining low material and low energy consumption.

Most of the current smart structures are made of stiff members connected and actuated by separate active devices based on energy intensive morphing principles, i.e., electromechanical devices for energy standby, sensing and motor drive functions. Recent developments in the field of soft robotics are based on pneumatically actuated smart materials that offer interesting performance, together with shape-changing complexity. Some of these devices are made of a cylindrical tube or bladder surrounded by a braided sleeve with a constant pitch angle and generate contraction or rotation during pressurization.[5] Conolly et al.[9] and Martinez et al.[10] have developed and manually produced pneumatic shape changing materials with an architected tube-like structure where stiff fibres (Kevlar or cellulosic) are helically patterned around a moulded elastomer tube. The response of the actuators depended on the winding angle of the stiff fibers within the soft matrix and their distribution along the tube length. However, the response of those tubular devices depends on the applied pressure, and that may be questionable for weight minimization purposes[11] and applications in severe environments, in which the energy consumption should also be minimized. In specific contexts such as space exploration, priority is given to autonomous actuation and self-adaptation to the environment.

Derived from simplified 2D bilayers or asymmetric lay-ups of plant tissues, passive structural actuator materials made of polymers and composites can undergo significant shape changes by leveraging the mismatch in coefficient of thermal expansion (CTE) or coefficient of hygroscopic expansion (CHE) and structural anisotropy.[3] Currently, additive manufacturing is a key process to control the material arrangement and the related mesostructures of these responsive materials. In 2013, 4D printing techniques have been introduced.[12] 4D printing involves the development of programmatic spatio-temporal actuation (shape change, properties change, color…) based on printing multi-scale and multi-materials architectures activated by external stimuli. With 4D printed structures, the entire actuator can work as a computational resource for both perception and action control; this enables more robust, faster and more efficient designs of artificial actuators.[11] 4D printed devices differ from conventional mechatronic actuators, as they require less intensive central processing to achieve complex continuous motion.[13] It is also now widely recognized that 4D printing is a major tool for biomimicry design and meets the challenges of extreme environments, especially when autonomous shape changing is required.[14] The material programming principles of 4D printed and biomimicry devices rely on the physical properties of materials and their arrangement on several scales,[15] on the residual stresses induced during the printing step[16] or the internal stresses revealed during environmental stimulation.[12]

However, the mechanical performance of 4D printed materials and structures is currently limited, due to moderate stiffness and thus very low force generation.[17] The combination of soft with structural/load bearing materials is of high interest, but still rarely proposed to fill the gap in the bioinspired structural autonomous morphing landscape.[3] Laminated composites in 4D printing can be assembled to address multiple functional requirements such as shape transformation, but also structural integrity.[18] Wang et al.[19] and Le Duigou et al.[20] have proposed 4D printed shape change materials based on stiff continuous carbon fibres that reinforce a compliant polymer (PolyAmide 6.)l (cCF/PA 6-I) matrix with reversible thermal or electro-thermo-hygro actuation. Although complex and large shape changes are obtained, high stiffness under the thermal stimuli is preserved because of the carbon fibre stiffness and anisotropy. Once more, while the primary focus of investigation in 4D printed structures is the ability to change shape, the resulting force generated is seldom evaluated, despite its crucial role as a working mechanism.

Most 4D printed structures configurations have an initial planar cantilever (2D) shape that transforms into a 3D one during actuation.[21] However, a tubular-like architecture can provide 50% more work than a planar cantilever counterpart under environmental changes.[22] Lott and Bixbee[6] indicated that 2D bilayer cantilevers produce large deflections but little force, whereas bilayer materials with a 3D helix configuration can provide rotary motion with only small linear displacements and generate sufficient work to support external devices. Recently, Van Manen et al.[23] have introduced a novel reconfiguration concept consisting of switching from an initial 3D shape to a 3D transformation based on 4D printed reconfigurable tubular polymer metacomposites.

The present work aims to describe the design and characterization of a novel programmable 4D structural metacomposites that overcome bottlenecks of current smart structures (energy consumption and lack of autonomy). Based on a top-down biomimicry approach and 4D printing, we combine stiff continuous carbon fibres and a compliant polymer to achieve 3D-to-3D shape changing capabilities activated by thermal variation. Initial shapes in the form of tubular and helicoidal bilayered metacomposites are printed to allow the original 3D-to-3D transformation. The programming stage entailed controlling the mesostructure and overall architecture. The mesostructure of the 4D printed metacomposites is dictated by the architecture of the active layer (length, external and internal diameter), the pattern of the composite deposition (e.g., passive layer angle, composite surface fraction, passive to active layer ratio) and the overall architecture (length to width ratio and the transition from tube to a multistrand helix). The influence of these parameters over the thermally induced rotation within a large thermal stimulation (20–160 °C) is evaluated and discussed. Blocked torque measurements are also done to complete the investigation of the structural morphing under operational conditions where shape change is carried out together with load bearing. This new class of functional metacomposites is then compared to current smart materials in terms of energy density which defines the potential of rotation combined with the load bearing ability. Finally, a proof of concept of a tubular autonomous solar tracker is proposed.

2. Novel Metacomposite and its Behaviour

2.1. Natural Fibre Microstructure as a Source of Inspiration for Novel Shape-Changing Materials

Most of the current smart structures consist in complicated assemblies that are prone to failure while their morphing principles rely on energy intensive paradigm. These are two limitations for their application in severe environment like space exploration (**Figure 1**- Step 1). To lever these bottlenecks appropriate

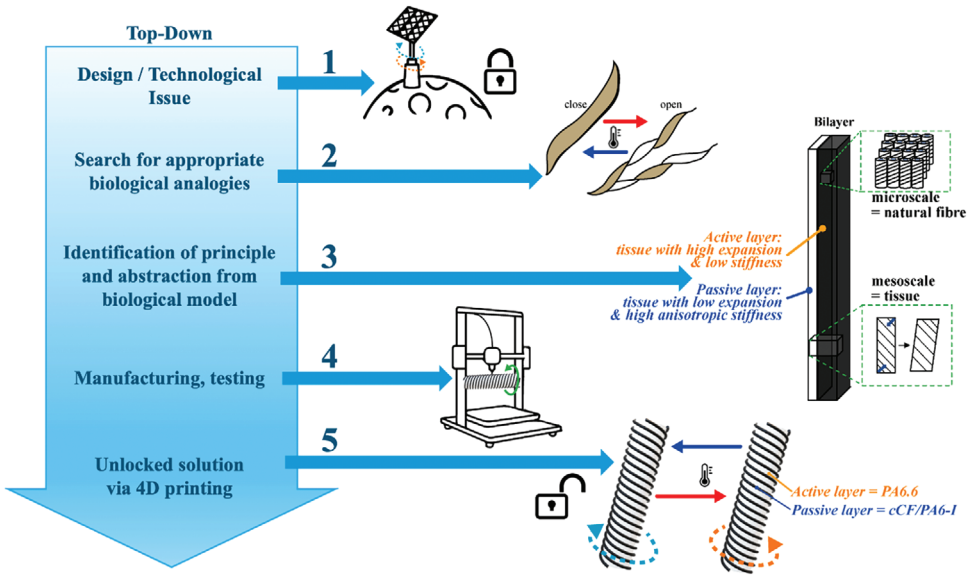

Figure 1. Diagram of the top-down approach proposed in this study to unlock lack of autonomy and energy consumption of current smart structures (step 1). Inspiration lies in the moisture-induced seed dispersion mechanism (step 2). The area of interest is at the level of the fibre cell wall scale, in which the fibres are architected in a tubular shape with stiff cellulose microfibril winded around a compliant polysaccharide matrix (step 3). Adapted from.[10,24] Differential expansion between the polysaccharide matrix and the aligned cellulose microfibrils generate rotation of the cell-wall assembly, i.e., the whole fibre. A novel rotative printer is designed and built to fabricate the 4D bioinspired printed bilayer tubes (step 4). Those tubes are made of an active layer of PA6.6 polymer that mimics the compliant polysaccharide matrix of the natural fibres and generates a large thermal expansion (c). A passive layer composed of high-end structural material is deposited. The load-bearing materials is made with stiff continuous carbon fibres embedded in a compliant polyamide matrix (cCF/PA6-I). The winding angle of the cCF/PA6-I mimics the MicroFibril winding Angle (MFA) found in natural fibre cell-wall. The concept is generated by rotationally reconfigurable and thermally induced composite structures, printed in 4D (step 5).

biological analogues are researched (Figure 1- Step 2). Biological hydraulic actuators such as the *Cytisus scoparius* can generate an autonomous helical morphing displacement triggered by temperature or/and moisture changes (Figure 1- step 2). The hierarchical and multiscale material organisation within these biological actuators is the key factor in generating the movement.[1,2] The homogenised mesoscale (i.e., ply scale or tissue scale) based on a planar architecture is currently the main source of design inspiration for bioinspired materials due to its simple architecture and fabrication.[25] At the mesoscopic scale, the helix actuation for the pod opening results from differential shrinkage/expansion between layers and thus the different thermal or hygroscopic internal stresses between the tightly bound layered tissues.

Biological actuators are far more complex than simple homogenised materials. Material organisation is based on hierarchical and multiscale architectures of tissue (Figure 1- step 3). Layered tissues are composed of hexagonal multiscale cell-walls, which are named as fibres. The latter are organised in bundles, held together by a middle lamella. Each fibre is tube-like architected, with concentric layers composed of stiff cellulose microfibrils embedded in a compliant polysaccharidic matrix of pectins, hemicelluloses and lignin.[26] Once wet or dried, a single natural fibre delivers chiral twisted actuation in a counter-clockwise direction;[27] the actuation is due to the helical cellulose microfibrillar pattern and the hygro-expansion of the amorphous matrix in the inter-lamellar layers.[28] It is now well established that the S2 layers control their hygroexpansion and mechanical properties through their internal organisation based on the cellulose microfibril winding angle (MFA), the fibre surface ratio and their composition.[1,26,27,29]

As an example, a bundle of a loblolly pine fibres (*Pinus taeda*) (10< Length <25 mm and diameter ~50 µm) that contains three to ten single fibres show ~2 reversible revolutions per cm length in direct proportion to the change of moisture content (0-90%RH). A single hemp fibre (Length ~30 mm and diameter ~20 µm) subjected to a moist environment from 10 to 80%RH provides a twisting actuation of 25°,[27] while keeping its longitudinal stiffness between 10 and 20 GPa.[27] This allows an efficient combination of shape-changing properties and torque generation and leads to structural actuation. According to Plaza et al.[30] and Jakes et al.,[31] the bundles generate from 10 to 25 Nm kg^{-1} of specific torque during both twisting and untwisting, confirming previous work published in the Seventies.[32] These biological structures show therefore a structural actuation potential that combines performance of shape changing and force generation.

Their relationship between architecture and performance rules the programming step. It can be conceptualised into a novel design of a bilayer multimaterial in cylindrical shape that provides such structural actuation. The proposed concept of 4D printed tubular bilayer composite can be considered as novel evolution of the McKibben-like structure. In addition, this bioinspired concept may be used as an analogue for reverse biomimicry, as it provides the opportunity to have better insights of the morphological function of the biological structure itself. This point is however outside the scope of the present work and will not be discussed further.

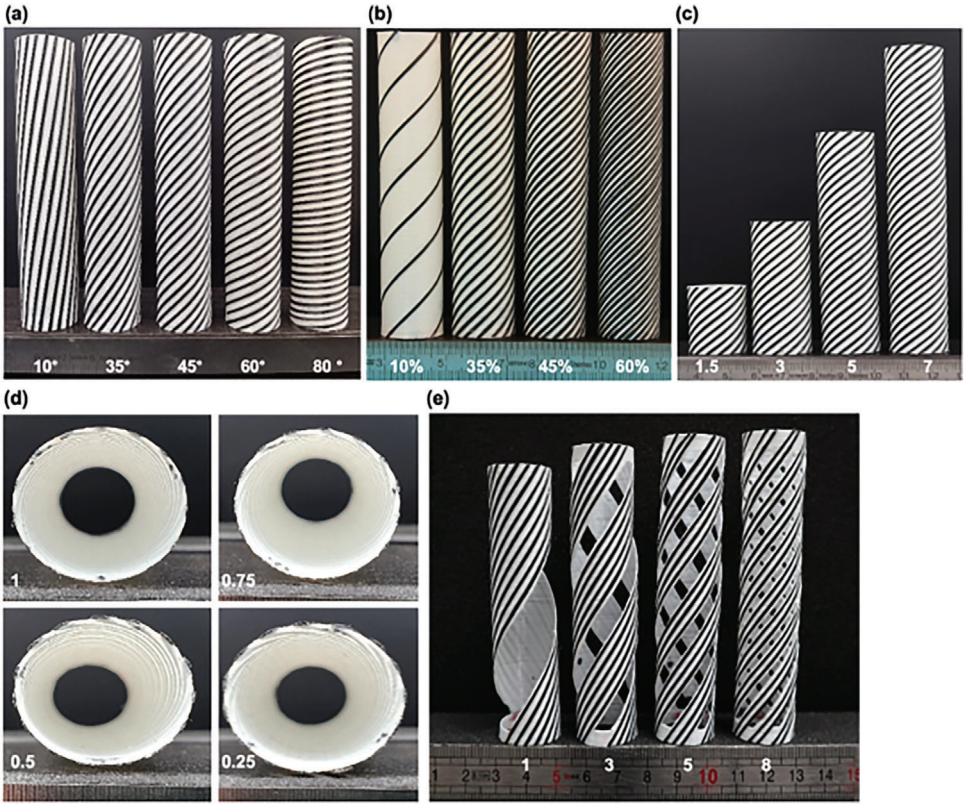

Figure 2. Images of the 4D-printed tubular bilayer samples according to their mesostructural configurations: a) Passive Layer Angle or PLA (composite layer) from 10 to 80°, b) Passive layer Surface Ratio (composite layer) for PSR from 10 to 60%, c) ratio of length to width diameter (L/w) from 1.5 to 7, d) thickness ratio of passive to active layer (tp/ta) (composite to pure polymer layer) from 1 to 0.05 and e) strand number (N) from 1 to 8. The latter helix configuration corresponds to PLA = 33.5°, PSR = 20%, tp/ta = 0.25, L/W = 5.

Here we consider a thermally expansible polyamide matrix (in white in **Figure** 2a–e) that mimics the polysaccharide matrix of the natural fibre cell walls. This is the active layer of our assembly. Stiff continuous carbon fibres cCF/PA6-I (in black in Figure 2a–e) reinforce the polyamide matrix tube and are applied to mimic the cellulose microfibril.

Programming the actuation of the metacomposite can be achieved by controlling either the mesotructure or the global architecture. The mesostructure of the 4D printed metacomposite is parametrised in terms of passive layer angle (Figure 2a), passive layer surface ratio (Figure 2b), tube length to width ratio (Figure 2c), internal to external diameter ratio (Figure 2d), and number of strands that divide the tube to produce a helical architecture (Figure 2e). These original features allow to control the programming step of the 4D printed metamaterial. Further description of the helical production is proposed in the Material and Methods section.

The ratio of the longitudinal stiffness between the passive and active layers (Ep/Ea) are a critical parameter for describing the shape changing of the bilayer assembly stimulated by thermal or hygroscopic loading.[33]

The active layer in the biological structure is assumed to be the S2 layer. The S2 is in essence responsible for both the stiffness and the hygroexpansion of the natural fibre due its thickness and its microstructure (i.e., its cellulose content and microfibril angle).[34] However, the definition of the passive layer may be more complex due to the intricate architecture of such biological material. Thus, the stiffness ratio of the natural fibre itself is unknown, even if the stiffness ratio of the component ($E_{cellulose}/E_{polysacharide}$) can be assumed to be around 200 without taking into account the architecture in the cell wall. The stiffness ratio (Ep/Ea) of the bioinspired multimaterials component (cCF/PA6-I and PA6) is within a similar range ($E_{CF/PA6\text{-}I}/E_{polymer}$ ~200).

Finally, two macroscopic arrangements are compared in this study: the tube and the helix. The helix is created by appropriately cutting out the matrix material between strands of metacomposite material.

2.2. Programming the Rotative Shape Changing Behaviour of the Bilayer Tubular/Helicoidal Metacomposites with the Bioinspired Architecture

The temperature-induced shape-changing behaviours of the 4D printed tubular metacomposites are evaluated versus the architectural and geometric parameters described above. A large range of temperature has been selected, from 20 to 160 °C; these values include daily terrestrial temperature changes, but also more extreme environmental variations existing in space. Two extreme conditions are evaluated to describe the shape changing behaviour: i) free rotation or free stroke, in which no external

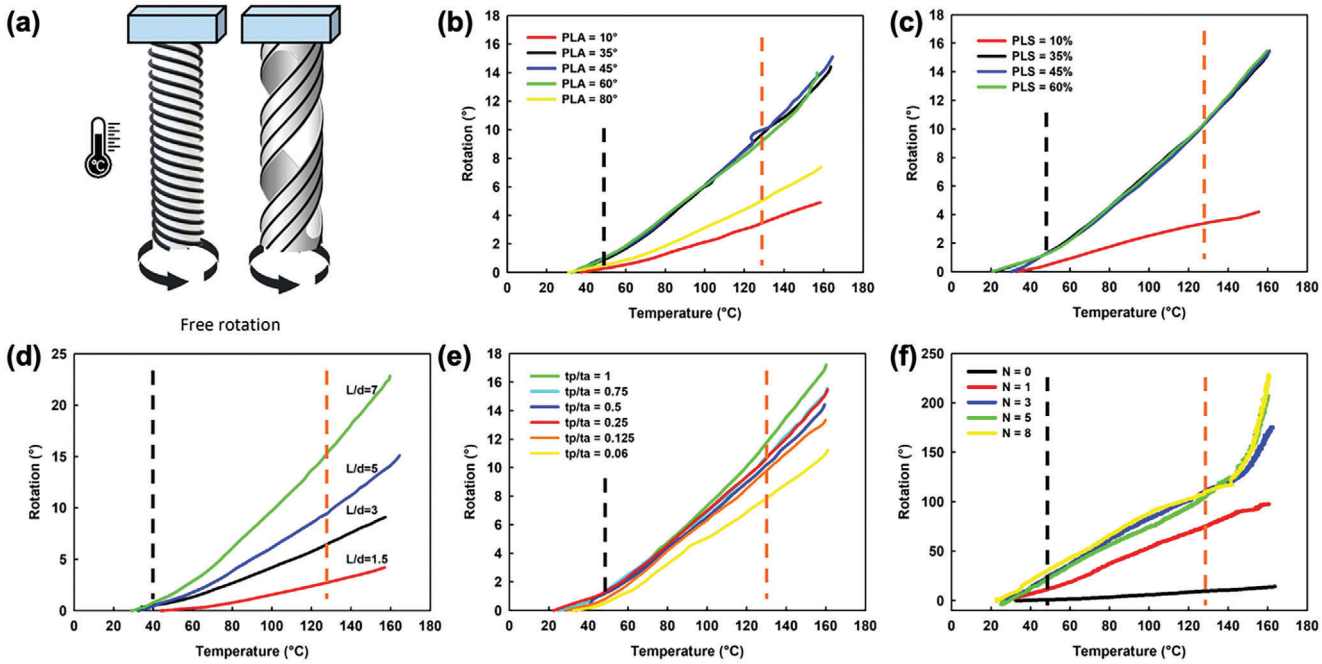

Figure 3. a) Schematics of the 4D-printed tubular and helical bilayer samples showing the free rotation test. One edge of the sample is clamped and the rotation versus the temperature is measured close to the sample. b) Passive Layer Angle for PLA of the composite layer from 10 to 80°, c) Passive layer Surface fraction (composite layer) for PLS from 10 to 60%, d) ratio of length to width diameter (L/d) from 1.5 to 7, e) thickness ratio of passive to active layer (tp/ta) (i.e., the composite versus the pure polymer layer) from 1 to 0.05 and (f) number of strands N from 1 to 8. The latter helix configuration corresponds to PLA = 33.5°, PSR = 20%, tp/ta = 0.25, L/d = 5. Orange dotted line represents the Tg of the active inner tube while black dotted line represents the Tg of the passive outer composite layer.

mechanical loading is applied. This condition allows to assess the design space in terms of displacement in non-operational or no-loading conditions (**Figure** 3a–e). The second condition is ii) blocked rotation (**Figure** 4a–e). The latter does not allow any motion and provides insights into the maximal torque generated and the boundary of operational conditions.

The free rotation of the tubular metacomposites is recorded when one edge of the sample is clamped. Unlike McKibben pneumatic tubular actuators that show complex nonlinear behaviour when the pressure is applied,[13] the different configurations of our 4D printed tubular metacomposites exhibit a quasi-linear behaviour. Therefore, the mesostructure of the passive layer (its composite angle, orientation and surface fraction) or the length to diameter ratio of the sample do not affect the global morphing behaviour (Figure 3a), even if their actuation performance is drastically altered. This remarkable feature makes these tubular metacomposites suitable for applications involving thermal control and leads therefore to an easier prediction of their behaviour for accurate positioning. This point will be further discussed in the last section of the article. Looking carefully at the morphing behaviour (Figure 3b–e), one can notice a slight slope change at 45 °C (the red dotted line on Figure 3), which corresponds to the glass transition temperature (Tg) of the PA6 polymer of the active layer being the inner tube, and thus to the drastic change of the CTE and tensile modulus. The effect of temperature over the properties of the passive layer composite appears to provide a minor influence on the global rotation, as the restraining effect induced by the longitudinal mechanical properties is only slightly altered by temperature.[25]

Changing the architecture from a tube to a helix defined by its number of strands (1<N<8) leads to a drastic modification of the morphing behaviour, especially at temperatures above 140 °C. This prevents the use of these metacomposites (with the presented materials) at those environments. The larger the number of strands, the more the mechanical behaviour becomes nonlinear. In these conditions, the shape change also becomes irreversible when the temperature decreases.

Under operational conditions, the 4D printed tubular metacomposite is subjected either to environmental loadings (e.g., change in temperature) and/or external mechanical loading to support any device. Here we have considered an extreme condition in which no rotation is allowed, so that the upper limit of the operational conditions can be identified (**Figure** 4a). The blocked torque behaviour observed in all the meso-architecture designs is similar (Figure 4b–e). The rotation starts at ~40 °C, which corresponds to the Tg of the active layer (inner tube). The linear portion is restrained over a moderate range of temperature and is then followed by a nonlinear portion until the maximal torque is reached. The maximum torque always appears at the same temperature range around 125 °C and may depend on the type of polymer used. At this temperature range, the continuous carbon reinforced/PA6-I passive layer undergoes a modification of its transverse and in-plane shear behaviour due to the onset of the glass thermal transition.[25] The torque finally decreases until the maximum testing temperature is applied.

In Figure 4d, the specific torque of metacomposites with different length to diameter ratios are plotted as a function of temperature. Although the actuation behaviors are generally

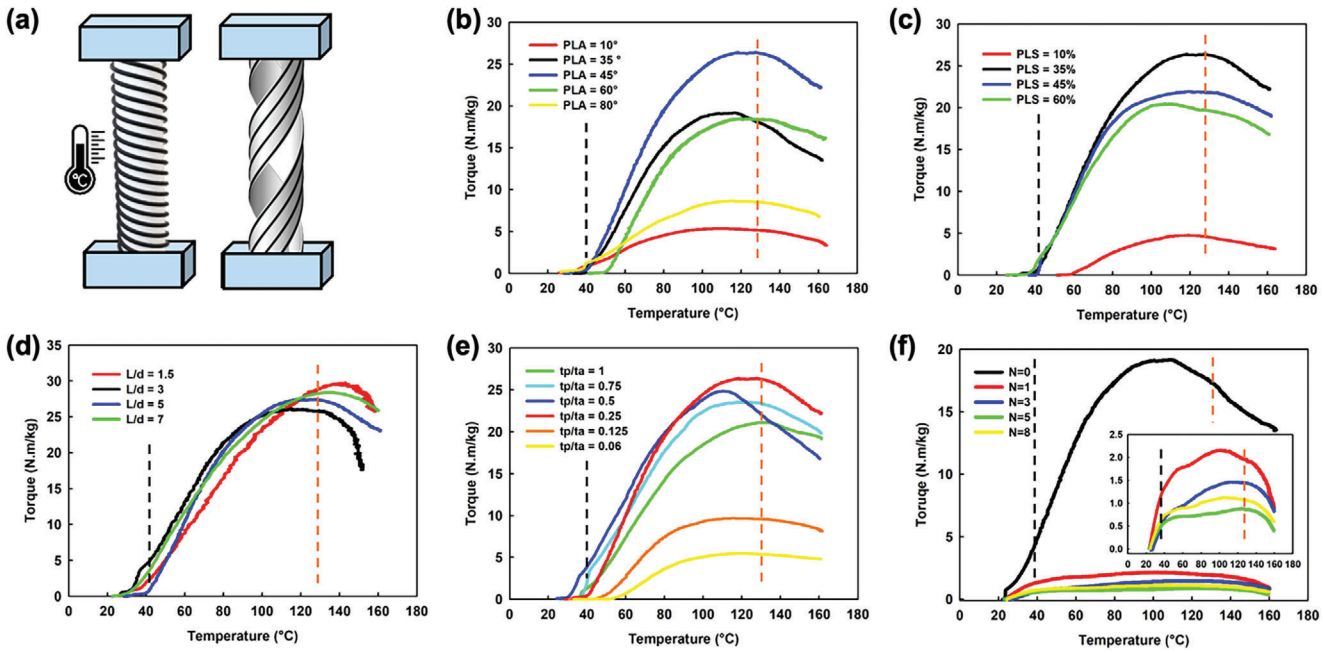

Figure 4. a) Schematics of the 4D-printed tubular and helical bilayer samples (N = 2) describing the blocked torque test. Both edges of the sample are clamped and the torque versus the temperature close to the sample is measured. b) Passive Layer Angle or PLA of the composite layer from 10 to 80°, c) Passive Layer Surface fraction (PLS) of the composite layer from 10 to 60%, d) ratio of length to diameter (L/d) from 1.5 to 7, e) thickness ratio of the passive versus the active layer (tp/ta) (i.e., composite to pure polymer layer) from 1 to 0.05 and f) strand number N from 1 to 8. The latter helix configuration corresponds to PLA = 33.5°, PLS = 20%, tp/ta = 0.25, L/d = 5). Orange dotted line represents the Tg of the active inner tube while black dotted line represents the Tg of the passive outer composite layer.

similar, slight irregularities can be observed. Indeed, the data plotted is representative of the average behaviour of each batch and not of all the samples. This may introduce a bias, particularly at high temperature where an unstable phenomenon may occur.

The estimated values of creep, i.e., the difference between the maximum torque and the torque at the maximum temperature are shown in **Table 1**. The time scale for the evaluation of creep is kept constant (~3.5 min) between all the samples. The analysis is done within a similar temperature range (between 125 and 160 °C) with constant kinetic of temperature increase (~10 °C/min). The thermally-induced creep during the blocked rotation is clearly due to the viscoplastic behaviour of the polymer and the internal re-arrangement at the polymer chain scale within the passive layer. The mesostructure of the passive layer (angle and composite surface ratio) affect the creep of the 4D printed tubular metacomposites. A lower angle and composite surface ratios lead to lower in-plane shearing properties in the passive layer and thus generate larger deformations in the matrix.

The transformation of the 4D printed tubular configurations into helicoidal metacomposites leads to a dramatic change of the blocked torque behaviour (Figure 4f), no matter the number of strands adopted. Between 25 and 55 °C the torque increases linearly, then a moderate increase of the torque is observed from 55 to 125 °C due to the stiffness reduction of the active layer. The increase of passive layer content (continuous carbon fibre composites) however increases the stiffness, so that the maximum torque can be reached around 125 °C, which corresponds to the Tg of the composite filament. Finally, between 125 and 160 °C the torque

Table 1. Evolution of the creep during the blocked torque measurements in the temperature range of 125–160 °C as a function of the passive layer angle PSR = 45°, tp/ta = 0.25 (ta = 0.4, tp = 0.1 mm), passive layer surface ratio PLS = 35% and strand number PLA = 33.5°, PLS = 20%, tp/ta = 0.25, L/d = 5. The time considered in the analysis of creep is constant (~3.5 min).

Passive Layer Angle (PLA °)	Creep (%)	Passive layer surface fraction (PLS %)	Creep (%)	Passive to active layer thickness ratio (tp/ta)	Creep (%)	Length to diameter ratio (L/d)	Creep (%)	Strand number	Creep (%)
10	29	10	35	0.06	12	1.5	13	0	26
35	26	35	14	0.125	16	3	14	1	30
45	16	45	16	0.25	16	5	16	2	36
60	14	60	15	0.5	18	7	10	3	46
80	21	-	-	0.75	16	-	-	5	46
–	–	–	–	1	10	–	–	8	56

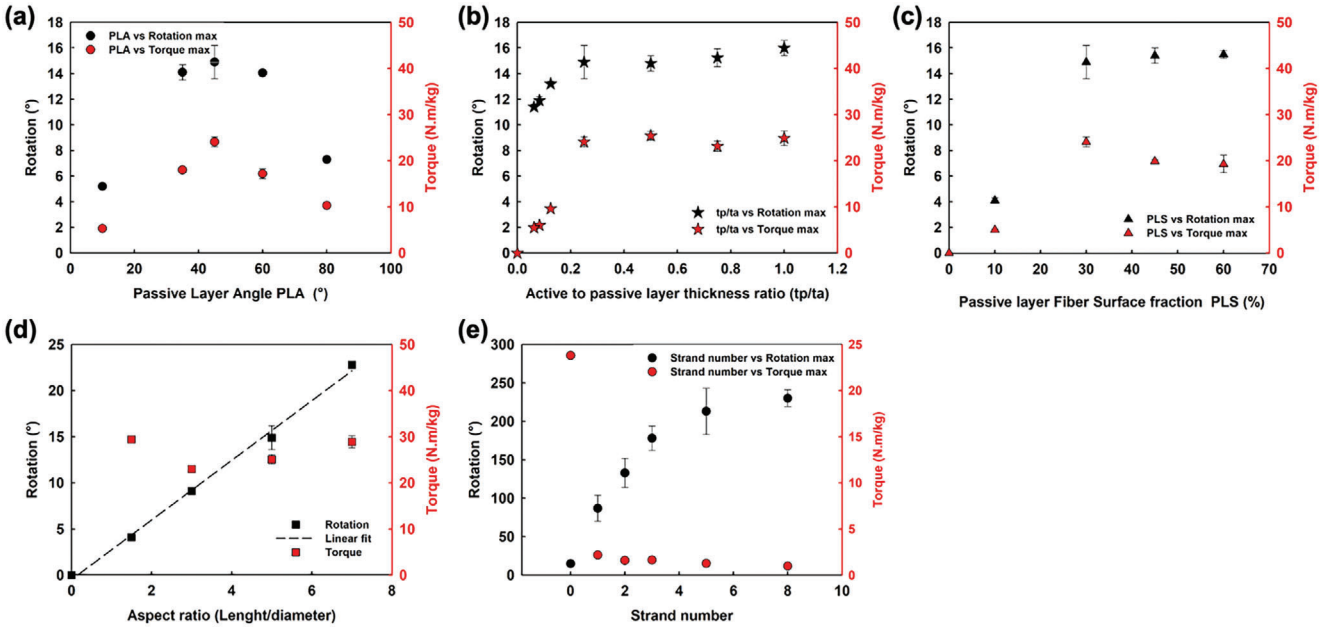

Figure 5. Evolution of thermally induced rotation and specific torque as a function of the passive layer angle (PLA) a), passive to active layer thickness ratio (tp/ta) b), Passive Layer Surface fraction (PLS) c), tubular length/diameter (L/d) ratio d) and strand number e).

drops drastically, and the decrease depends on the mesostructure parameters adopted for the different metacomposites (Table 1). Again, the thermo-induced creep mechanism decreases the internal thermal stresses by irreversible deformation of the strands; the latter is observed during unloading.

2.3. Evaluation of Morphing Properties as Programming Tool

Inspired from the architecture of the natural fibres, the mesostructure parameter and the geometry of the 4D printed tubular and helicoidal metacomposites enable the programming of wide range of specific rotations and/or torques. Those performance are identified from the morphing response (Figure 3b–e and Figure 4b–e) in terms of responsiveness, i.e., amplitude (maximal rotation) (**Figure 5**a–d) and reactivity (**Table 2**). The latter is indicative of the kinetic response (speed of rotation) under free motion and is expressed in °/°C. Reactivity expressed in °/min is proposed in Section S1.4 (Supporting Information) so that time to reach a targeted rotation can be calculated (within the proposed temperature range and kinetic).

The specific blocked torque corresponds to the maximum torque divided by the weight of the sample required to maintain a zero-rotation angle, when the thermal stimulus is applied.

The passive layer angle (PLA) that can be stated to act similarly as cellulose microfibrillar angle (MFA) is a key parameter in natural fibres to ensure their biologically programmed functioning. Low MFA in hemp or flax fibres generate large stiffness and lodging ability of the plant stem, while large MFA values bring toughness to coir fibres and related mesocarp. Here, the Passive Layer composite Angle (10, 30, 45, 60 and 80°) implies a non-monotonic variation of the responsiveness, reactivity and torque. The range of rotation angles varies from a factor of ~4 when the angle is changed from 10° to 45°. The 45° angle rotation is the maximum value for a deposition angle of 45°, which is common for tubular based actuators.[13] The stiffness ratio between the longitudinal and transverse directions is actually controlled by changing the PLA; the variation of the stiffness ratio induces

Table 2. Morphing kinetic or reactivity (slope of rotation versus temperature for the various mesostructural parameters (PLA, PSF, tp/ta) and geometrical consideration (L/d and strand number).

Passive Layer Angle (PLA °)	Reactivity or speed of rotation [10^{-2}°/°C]	Passive layer surfaces fraction [PLS %]	Reactivity [10^{-2}°/°C]	Passive to active layer thickness ratio [tp/ta]	Reactivity [10^{-2}°/°C]	Length to diameter ratio (L/d)	Reactivity [10^{-2}°/°C]	Strand number	Reactivity [10^{-2}°/°C]
10	4.0 ± 0.2	10	3.5 ± 0.3	0.06	9.0 ± 0.2	1.5	3.4 ± 0.3	0	10 ± 1
35	10.7 ± 0.6	35	11.8 ± 0.2	0.125	10.3 ± 0.4	3	7.1 ± 0.1	1	64 ± 1
45	10.8 ± 0.3	45	12.2 ± 0.4	0.25	11.8 ± 0.2	5	10.8 ± 0.3	2	100 ± 4
60	10.7 ± 0.2	60	12.0 ± 0.1	0.5	11.4 ± 0.6	7	18.2 ± 0.2	3	107 ± 3
80	6.0 ± 0.2	–	–	0.75	11.0 ± 0.1	–	–	5	96 ± 1
–	–	–	–	1	13.8	–	–	8	112 ± 4

a transition from tensile fibre dominated properties at low PLA, to fibre/matrix and matrix in-plane shear.

The passive to active layer thickness (tp/ta) ratio affects the global stiffness of the tubular bilayer and its morphing performance therefore, with a non-monotonic trend for both rotations and torques. An increase of the thickness ratio from 0.06 to 1 implies a 30% increase of rotational shape changing, a 53% increase of rotational kinetic and almost 450% of the specific torque. As a consequence, the tp/ta ratio is the first parameter to consider for programming the torque, rather than the shape change. Above a tp/ta value of 0.25, the morphing performance is almost constant; this indicates a clear limit for the design space.

For a fixed passive layer angle, the Passive layer surface fraction (PLS), i.e., the composite surface fraction, is also a mesostructure parameter that controls the in-plane stiffness of the passive layer, as well as of the global structure. An increase of PLS improves the responsiveness, the reactivity and the specific torque until constant values of those metrics are reached for PLS ~30%. Beyond this point, the global morphing performance is almost unchanged and adding more carbon fibres does not modify the behaviour. On the contrary, adding more carbon fibres will generates higher weights (d_{PA} = 1.15 versus $d_{carbon\ fibre}$ = 1.75) and larger environmental footprints. At lower PLSs, larger creep is observed for the blocking torque due to the significant contribution of the polymer over composite fibre materials. As a consequence, a fibre surface fraction of 30% appears to be optimal for designing the 4D tubular metacomposites.

The length to diameter ratio (L/d) from 1.5 to 7 linearly amplifies the rotation angle from 5° to 24° and the morphing kinetic by a factor 6 (see Table 2). The specific torque appears not to be significantly affected by the length to diameter ratio, with values ranging between 25–29 N.m/kg (Figure 5d). This may be due the geometrical stiffness of the tube that is reduced with the increase of L/d ratio. The Length /diameter (L/d) of the 4D printed tubular metacomposites produced in this work is limited by the size and the resolution of the printer developed, and is therefore significantly lower than our source of bioinspiration. The L/d of flax fibres is around 1500.[34] A linear increase of rotation with L/d paves however the way for a relevant scale-up printing process to obtain shape changing materials with larger responsiveness and reactivity. For example, the 4D tubular metacomposite should be close to one meter long with similar diameter and torque, if a 180° rotation is targeted.

Another way to increase the rotation is found by switching from the tubular architectures to helical ones with various number of strands (Figure 5e). In this way, the responsiveness of the rotation can be multiplied by 5–15 by increasing the number of strands and the reactivity versus the temperature by factor of 6 to 12 (see Table 2).

However, this change of architecture leads to an overall decrease of the stiffness of the metacomposites, with a consequent dramatic reduction of the blocked torque by a factor of 12 to 24.

From a general perspective, the performance of the 4D printed tubular metacomposites developed here allows for a large range of rotation, torque and reactivity. The mechanical performance of these metacomposites is superior to those of our source of inspiration, i.e., natural fibres like hemp or wood (Figure 5). Indeed, a single hemp fibre subjected to a humid environment generates

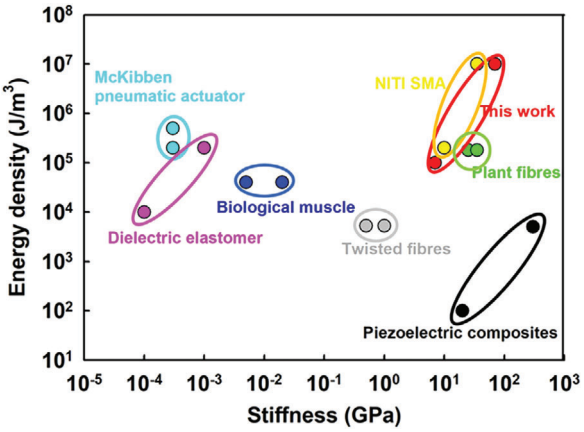

Figure 6. Ashby-type of plot of the energy density (J/m^3) as a function of the material stiffness. Stiffness for metacomposites and natural fibre corresponds to longitudinal tensile stiffness. The data extracted from the open literature are taken from.[10,11,36–38]

25° of rotation,[35] while wood bundles generate specific torques around 10 N.m/ kg while drying.[30] Interestingly, these values are larger than those of commercial electric motors that generate up to 6 N.m/ kg,[30] carbon nanotube yarns in electrolyte solutions (2.4 N.m/kg[30]), wax-filled carbon nanotube yarns (8.4 N.m/kg[30]) or of McKibben like paper/elastomer actuators (1.9 N.m/kg[10]).

It is interesting to consider the maximum work energy density as another metric to further assess the performance of these novel adaptive materials. This is defined as the area under the maximum torque–rotation curve. Work energy density gives an approximation of the volume needed by a specific actuator to generate a given amount of work. A trade-off between stiffness and energy density (J/m^3) of different smart materials and our metacomposites is mapped in **Figure 6**. Caution should be taken with stiffness values. Data for metacomposites and natural fibre are longitudinal tensile stiffness. However, beyond isotropic materials, most of data extracted from literature does not evidence the anisotropy of their properties. The longitudinal axis is relevant to evaluate as it will be the loading direction when a potential solar panel will be placed on the top of the tubular metacomposites.

The proposed 4D printed metacomposite concept outperforms most of the synthetic and fossil-based smart materials currently used for morphing or torque generation. It is also worth of notice that most of the synthetic smart materials are used for one main function (shape changing or torque), but they are rarely able to fulfil the two functionalities at the same time.

Biological materials like natural fibres combine compliant and stiff components in a complex architecture (Figure 6). This source of bioinspiration allows the metacomposites proposed here to provide promising trade-offs between energy density and stiffness thanks to the combination of a compliant material responsive to temperature (i.e., the active layer) with stiff anisotropic reinforcements (i.e., the passive layer). In addition, the large customisation possibilities offered by 4D printing through tailored mesostructures and architectures enlarge the design space of these novel metacomposites.

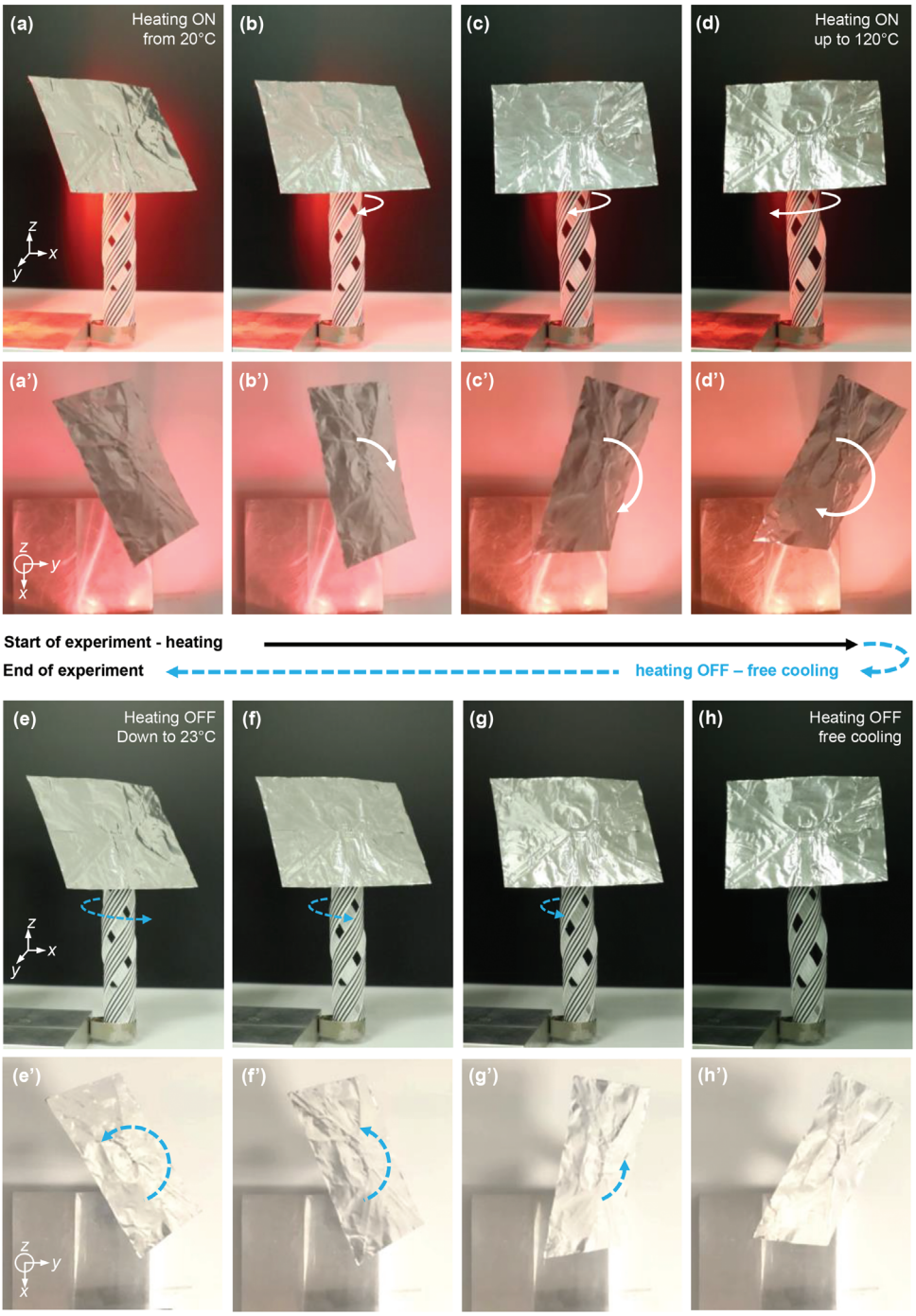

Figure 7. Passive solar tracker with a shape changing mast made with the helical metacomposite a). Experimental set-up showing the shape changing helical metacomposite (PLA = 33.5°, PSR = 20%, tp/ta = 0.25, L/W = 5, N = 1) topped by a simple metallic frame mimicking solar panels/reflectors. The tracker is seen in the (x; z) plane (from a to d) and from the top in the (x; y) plane (a' to d') during a 20–120 °C heating provided by the radiator. The part rotates less compared to the free actuation setup without any weight. Then radiant heating is turned OFF and the tested part is observed during free cooling down to room temperature in (x; z) plane (from e to h) and from the top in (x; y) (from e' to h'). The part rotates in the opposite direction towards the original position. Schematic view of a). Video clips are available in the Supporting Information.

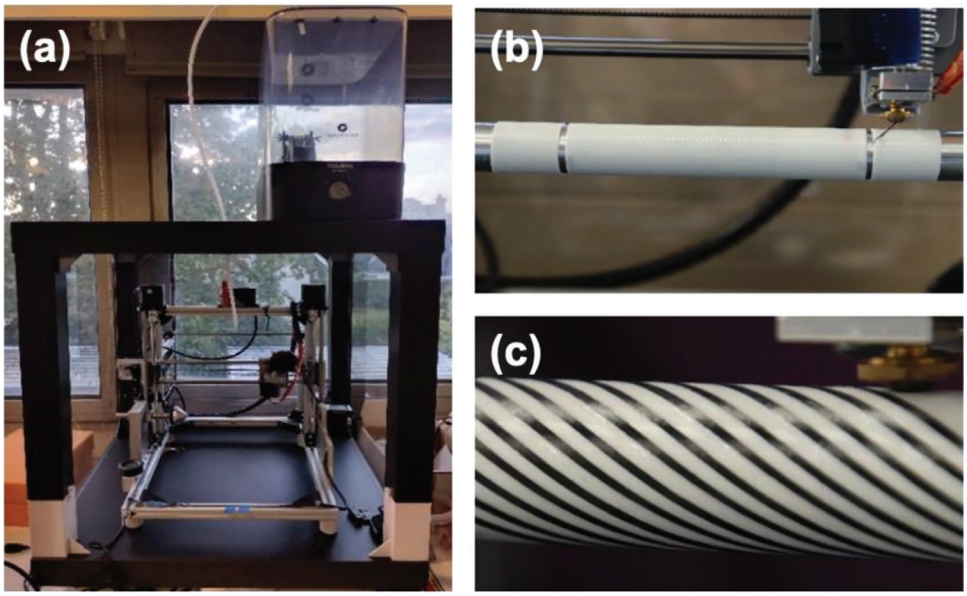

Figure 8. a) Schematic of the rotative printing process. To ensure high print quality, the printer was placed in an isolated chamber to reduce heat losses. The continuous Carbon Fibre reinforced Polyamide-6I composite (cCF/PA6-I) spool (in black) was, as the PA6.6 spool (in white), placed in a humidity-controlled box (RH = 10%). b) Once the PA6.6 inner tube (white) was printed using a conventional FFF printer, it was mounted on a rotative shaft. c) a Bowden-like extruder with a roller to feed the continuous carbon fibre-reinforced PA6-I filament (black) is used to print the passive layer onto the polymer inner tube.

2.4. Proof of Concept of Passive Solar Tracker/Reflector Based on the Programmable Tubular Metacomposite

Amongst extreme ambient conditions, the large temperature variations and remoteness typical of off-earth environments and deep-space missions are particularly severe and require designs of the infrastructure based on autonomous operating principles. Current smart structures like solar trackers are based on electromechanical paradigms implying energy for standby, sensing and motor drive functions. Future smart structures and materials for applications in severe environments will have to react autonomously and adapt to their surroundings within different time frames to reduce maintenance requirements and optimise their performance of use. Here we propose the tubular metacomposite to be used as a smart platform or mast for passive rotation actuation of a passive solar tracker subjected to photothermal effect from sun rays (**Figure 7**; Video S1, Supporting Information). This novel metacomposite may also be used in the manufacture of sustainable generic robots with reduced power supply for solar panel arrays with adaptive booms, deployable antennas, adaptive louvers, solar concentrator/shield or even for medical applications (adaptive stents...).

The main purpose of this paper is to provide a novel programmable shape changing metacomposite in terms of spatio-temporal actuation. This means that the design window is evidenced but the programming for a dedicated specification (e.g., rotation to follow a trajectory for heliotropism) is outside the scope the article. Under these conditions, AI-based algorithms via parametric or topological optimization should be relevant to identify the best mesostructure and architecture configuration taking into account their transient and stationary thermo-mechanical properties.

A helical configuration (N = 1) of the tubular metacomposite has been clamped to a metallic frame and placed at 10 cm from a 2×500 W radiant heater (Figure 7; Video S1, Supporting Information). The temperature variation towards 100 °C is monitored by a manual controller and a thermocouple located close to the sample. To mimic a solar tracker/reflector we have built a simple metallic frame (mass = 2.73 g) representing the solar cells assembled on top of the tubular metacomposite with mass = 2.24 g. The rotation is then triggered and reach a value close to 50°. As expected, this angle is slightly lower than the one that could be obtained from free loading conditions (Figure 2). The cooling is triggered by switching off the heater and the initial position is fully reached.

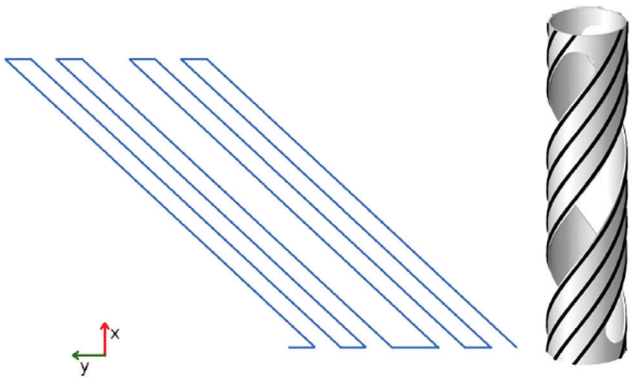

Figure 9. Programmed trajectories (left) and effective trajectories on the polymer tube (right).

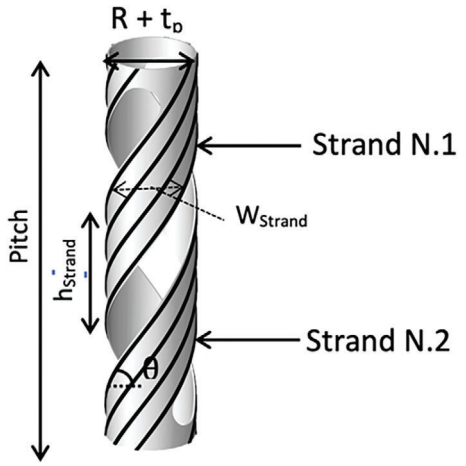

Figure 10. A schematic view of a helicoidal of metacomposite made with PA6 helix winded with cCF/PA6I Composites.

3. Conclusion

Current technological challenges lead material scientists, mechanical engineers and designers to provide solutions that reduce energy consumption and maintenance for devices and components operating in severe environments like for space exploration. For that, cross-disciplinar work through biomimicry and 4D printing is a required framework.

To overcome current limitation of smart (e.g., lack of autonomy and energy consumption), we have developed an original concept of 4D printed programmable tubular structural metacomposite with a 3D-to-3D shape changing capability activated by thermal variation. Our bioinspired device mimicked the tubular bilayer architecture of plant fibre cell wall that generates structural actuation with large rotational motions and high torque while being actuated. The presented concept has the inner tube layer made with PA6.6, a thermally responsive polymer acting as the active layer, similarly to the polysaccharide compliant matrix within a natural fibre. The outer layer tube or the passive layer is made with winded continuous carbon fibre/PA6-1 composites. This layer brings stiffness, actuation authority and directionality, similarly to cellulose fibrils in the natural fibre. The constitutive materials were used as an example that will be selected carefully depending on their thermomechanical properties and the environment.

Once subjected to a temperature variation between 20 °C and 160 °C, the 4D tubular metacomposite was able to generate both rotation responsiveness and reactivity, as well as torque at levels that could be tailored during the design and the printing steps. In general, the 4D tubular metacomposites showed encouraging performance levels in a similar range of shape memory alloys and even larger than the natural fibres from which inspiration was taken. Interestingly, they outperformed synthetic smart materials that are often designed for single tasks, morphing or torque like McKibben pneumatic tubular actuators or dielectric elastomers. Therefore, these 4D tubular metacomposites possessed a wide range of response programming through the customization of the mesostructure of the passive layer, their global architecture and can even be designed with a transition from full tubular to helical tubular with various numbers of strands. This opens the way to novel paradigmatic autonomous metacomposites for structural morphing, like autonomous solar tracker as suggested in this work.

Future work may focus on two different ways to extend our concept. The first is the programming of the structure using AI-based optimisation tools, so that heliotropic actuation may be systematically designed and produced. The second is the assembly of the metacomposites into complex metastructures with combined responses.

Table 3. Parametric data for the construction of the 4D printed helical metacomposites.

	1 strand	3 strands	5 strands	8 strands
L_{Strand} (mm)	113.6	104.9	104.2	103.9
W_{Strand}	70	23.3	14	8.75
N_F	14	5	3	2
PLS (%)	34.8	37.3	37.3	39.8
Helix length (mm)	92	99	102	103
Internal radius (R) (mm)			10.6	
Pitch (mm)			100	
θ (°)			56.6	
Thickness of the helix (mm)			0.4	

4. Experimental Section

Materials: PolyAmide 6.6 (PA 6.6) from Markforged is used as the thermal active layer. The mean coefficient of thermal expansion (CTE) measured by dynamic mechanical analysis (DMA, Q800 DMA from TA Instruments) in compression over a temperature range from −40 to 120 °C is 137 10^{-6} $°C^{-1}$. The glass transition temperature (Tg) of PA6.6 was measured by DSC to be 55 °C.

The thermal passive layer is a composite filament supplied by Markforged which consists of continuous carbon fibres (vf = 35%) embedded in a polyhexamethylene-isophtalamide matrix (cCF/PA6-I). The Tg of the PA 6-I matrix is 125 ± 2.5 °C. The cCF/PA6-I filaments have a diameter of 379, 8 ± 10.5 µm, while the porosity volume in the filament prior to printing was measured to be 1.85 ± 0.3%.[39] The mean CTE measured by the same devices as for PA6.6 over a temperature range from −50 to 200 °C is 50 10^{-6} $°C^{-1}$ for transversely and assumed to be negligible for longitudinally oriented cCF/PA6-I due to the carbon fibre properties.

3D printing and Manufacturing Parameters—Inner Tube—Active Layer: Prior to printing, the PolyAmide (PA6.6) filament was stored under vacuum for at least 48 h at 35 °C to remove sorbed moisture and to guarantee high print quality, and during printing in an airtight box (RH = 10%).

A conventional Prusa MK3S print device was used for PA6.6 printing. The. STL file of the hollow tube was designed using SOLIDWORKS Premium 2021 SP2.0 and imported to PrusaSlicer with which the.GCODE was generated. The nozzle's diameter and temperature were 0.4 mm and 250 °C, respectively. The bed temperature was set to 90 °C. The print speed was 60 mm^{-1} s, while the print direction was at 90° to the longitudinal axis to maximise the thermal expansion ability of the material.[23,40] The spiral vase mode was activated to avoid any seams along the tube, while keeping the print height at 0.2 mm. A calibration protocol was applied to determine a correction factor considering the difference between the programmed and the real extruded material quantity. The printer was placed in an isolated chamber to reduce heat losses.

Then, the PA6.6 polymer tube (white part in **Figure 8**b) is removed from the printing bed and then a thermal treatment of 2 min at 160 °C

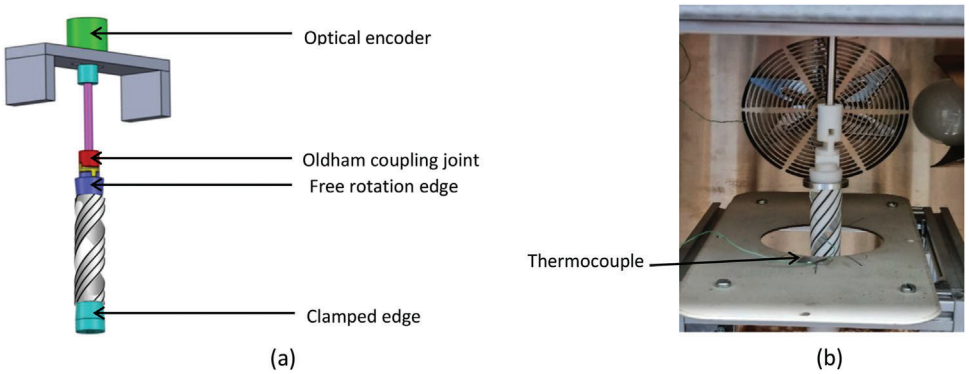

Figure 11. a) a Schematic representation of the rotation measurement of metacomposite under temperature variation b) Real experimental set up included into a programmable oven.

is applied to fully release the thermal residual stresses. Thus, the subsequent morphing is only triggered by the thermal internal stresses implied by the surrounding environment. Architecture of the tube is characterized before and after the thermal treatment.

3D Printing and Manufacturing parameters—Tubular Metacomposite Production: Composite winding through rotative printing for the passive layer Once the inner PA6.6 tube is printed, it is mounted on a shaft from an in-house designed 3D print device (Figure 8a,b), which is based on a Prusa I3. Then winding of continuous Carbon Fibre reinforced Polyamide −6I composite (cCF/PA6-I) (black elements in Figure 8c) is achieved. Open edge tube was used whatever the configuration of the mesostructure.

The supports were water jet machined and milled in aluminium and steel alloys to increase stiffness and reduce deformation during printing. The rotation of the shaft was achieved by a stepper motor, which enables the printing of complex patterns.

This motor acts exactly as the one that generates the displacement on the Y axis on a conventional printer and is controlled as such. The Gcode instructions representing the trajectories to be followed by the print head are hence written as if the polymer tube was a planar sheet. The rotation of the shaft, rather than a displacement of the Y axis, then translates these flat trajectories into the desired spiral pattern on the polymer tube. When writing Gcode instructions, it is therefore necessary to take this conversion into account, by programming trajectories such as those in **Figure 9** – left, to generate effective trajectories such as shown in Figure 9 – right.

Rotation has been facilitated using roller bearings to reduce friction problems. Like earlier custom printers developed in our lab, it has a Bowden-like extruder with a roller to feed the continuous fibre-reinforced filament and to reduce sudden pull when the nozzle pulls the filament. This resulted in better printing accuracy, especially at the edges of the samples.

The heater allowed printing at high temperatures, while an in-house designed flat nozzle with a diameter of 0.9 mm ensured the correct deposition of the composite on the PA6.6 layer through ironing effect.

The diameter of the tubular structure is defined so that it can be manually placed on a mandrel, held during the printing process without slipping and removed after printing.

The nozzle was heated up to 280 °C, while the shaft was not tempered. The layer height was controlled by a height sensor. To ensure high print quality, the printer was placed in an isolated chamber to reduce

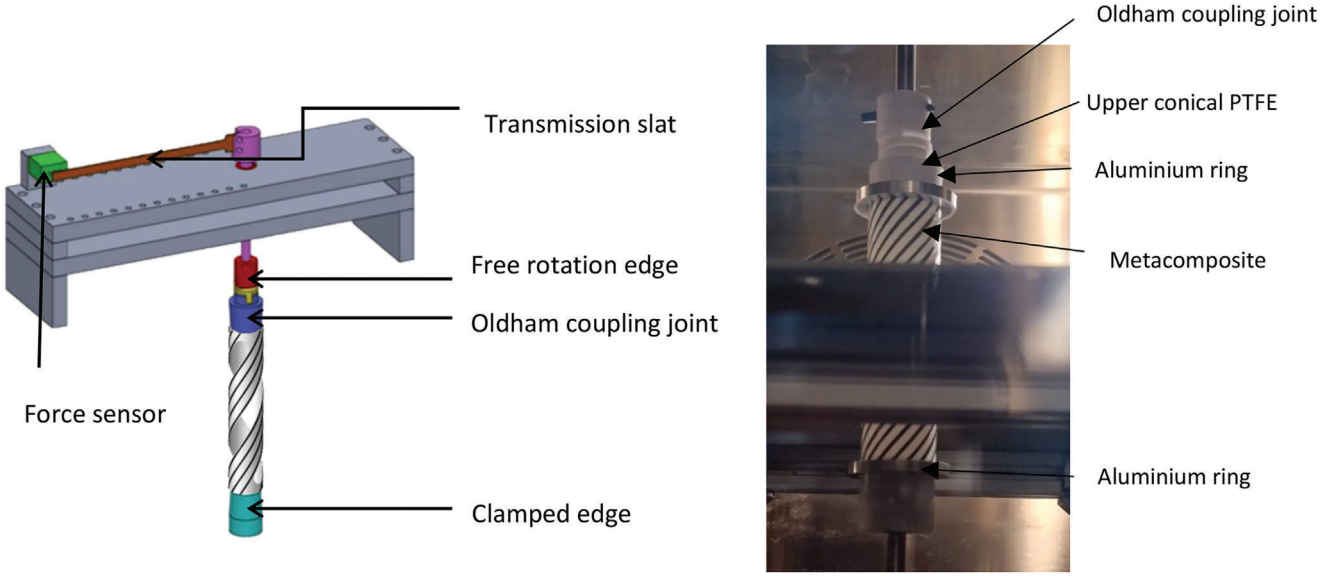

Figure 12. a) Schematic representation of the torque measuring devices. It consisted of an optical encoder. An Oldham coupling linked the optical encoder with the tubular sampler was mounted on conical supports made of PTFE. Two aluminium rings were further attached to the extremities of the sample. b) Image of the whole torque measuring device placed inside a heating chamber and applied to 4D metacomposite materials. A lever arm is connected to the sample by an Oldham coupling to measure the morphing force.

heat losses. The cCF/PA6-I spool was placed in a humidity-controlled box (RH = 10%) and the filament was pulled through a closed circuit into the print chamber to the print head (Figure 8a). The print speed of the composite was set to 5 mm^{-1} s. The programmed layer height was set to 0.5 mm, which corresponded to the previously set height of the PA6.6 (0.4 mm) plus the composite height (0.1 mm). The real print thicknesses of the PA6.6 and the composite were systematically checked by microscopic analysis. The Gcode file was generated using FullControl Gcode Designer, an open-source software for unconstrained design in additive manufacturing. The dependence of the geometric parameters (inner radius and thickness of active layer; surface fraction, width and angle of passive layer) on each other which is necessary for programming the print path was derived by trigonometric calculations (see Supporting Information).

3D Printing and Manufacturing Parameters—Helical Metacomposite Production: The helical structures (Pitch = 100 mm; R = 10.5 mm; t_p = 0.4 mm) are printed by changing the strand numbers as well as the strand height (h_{Strand}) (**Figure 10**). Again, open edge tube was used. Other parameters depend on those inputs parameters and are listed in **Table 3**. Strand number varies from 1 to 8. The printing parameters are kept similar with the tubes.

By modifying the the W_{Strand} and the L_{Strand}, the pitch as well as the fibre content must be modified. According to the test carried ou on tubes, a composite surface fraction of 35% allow to obtain the highest rotation when submitted to temperature variation. The number of composite filaments per strand N_F, has to be chosen to reach similar value of PLS. Pich, angle (θ) and the internal radius are kept constant (Table 3). The length of the strand is calculated as follows:

$$l_{strand} = 2 \times 180 \times \frac{h_{strand}}{\text{pitch}} \tag{1}$$

$$\theta = \arctan\left(\frac{h_{strand}}{l_{strand}}\right) = \arctan\left(\frac{\text{pitch}}{2 \times 180}\right) \tag{2}$$

$$L_{strand} = \sqrt{l_{strand}^2 + \left[2\pi\left(R + t_p\right)\tan\left(\theta\right)\right]^2} \tag{3}$$

The calculation of the PLS is proposed in Annex 1.

Characterization Methods—Microanalysis: A microanalysis of the printed material was performed to determine the thicknesses of the printed layers. The printed materials were polished and placed under a numerical microscope (Keyence VHX-7000) with different magnifications (×200 & ×500). Five images were used to determine the thickness parameters for the pristine and printed material.

Characterization Methods—Morphing Characterisation—Rotation Measurement: An in-house designed measuring device was used to record the rotation of the 4D printed materials (**Figure 11**a). It consisted of an optical encoder from Copal Electronics with a resolution of 0.345°. An Oldham coupling linked the optical encoder with the tubular sampler which was mounted on conical supports made of PFTE to minimise the friction of the system.

Two aluminium rings were further attached to the extremities of the sample to avoid possible sliding in vertical direction. Aluminium was chosen to keep the system as light as possible. The tubular samples were heated from room temperature to 160 °C within 13 min with a constant kinetic of ∼10 °C/min in an oven from Matair (Figure 11b). At 160 °C, the temperature was maintained for 2 min. The oven was then switched off and opened and the measurements maintained until the rotation had almost completely returned to zero. During sample testing, two thermocouples recorded the temperatures close to the tubular sample and in the oven (Figure 11b).

Characterization Methods—Morphing Characterization—Torque Measurement: The second measuring device was also in-house designed and contained a low-capacity S-beam force sensor from PM Instrumentation substituting the optical encoder and a transmission slat that served as lever arm. Its rated force and accuracy were 2N and 0.1%, respectively (**Figure 12**a). As for rotation measurements, the tube was mounted on conical PTFE supports (Figure 12b) and fixed with two aluminium rings to prevent vertical sliding. Heat temperature and time, and oven were the same as for rotation measurements. The couple was then calculated from the measured load and the lever arm applied.

Supporting Information

Supporting Information is available from the Wiley Online Library or from the author.

Acknowledgements

The authors wish to thank ESA OSIP platform (Contract No. ESA 4000133620) and IRT Saint Exupery for fundings. The authors acknowledge Quentin Le Paih for technical development and Julia Fernandez for her involvement.

Conflict of Interest

The authors declare no conflict of interest.

Data Availability Statement

The data that support the findings of this study are available on request from the corresponding author. The data are not publicly available due to privacy or ethical restrictions.

Keywords

4D printing, Biomimicry, functional composite

Received: March 11, 2024
Revised: June 12, 2024
Published online:

[1] P. Fratzl, R. Elbaum, I. Burgert, *Faraday Discuss.* **2008**, *139*, 275.
[2] P. Fratzl, F. G. Barth, *Nature* **2009**, *462*, 442.
[3] M. P. Jones, G. G. Murali, F. Laurin, P. Robinson, A. Bismarck, *Compos. Sci. Technol.* **2022**, *230*, 109792.
[4] C. Baley, *Compos. Part A Appl. Sci. Manuf.* **2002**, *33*, 939.
[5] G. M. Spinks, *Adv. Mater.* **2020**, *32*, 1904093.
[6] D. R. Lott, R. C. Byxbee, *Final Report* **1969**.
[7] P. Camilla, D. Izzo, *Bioinspir. Biomim.* **2013**, *8*, 9.
[8] C. Sanchez, H. Arribart, M. Madeleine, G. Guille, *Nat. Mater.* **2005**, *4*, 277.
[9] F. Connolly, C. J. Walsh, K. Bertoldi, *Proc. Natl. Acad. Sci. U.S.A* **2017**, *114*, 51.
[10] R. V. Martinez, C. R. Fish, X. Chen, G. M. W. Elastomeric Origami, *Adv. Funct. Mater.* **2012**, *22*, 1376.
[11] W. Liang, H. Liu, K. Wang, Z. Qian, L. Ren, L. Ren, *Adv. Mech. Eng.* **2014**, *12*, 168781402093340.
[12] S. Tibbits, *Architectural Design* **2014**, 116.
[13] M. Schaffner, J. A. Faber, L. Pianegonda, P. A. Rühs, F. Coulter, A. R. Studart, *Nat. Commun.* **2018**, *9*, 878.
[14] A. Mitchell, U. Lafont, M. Hołyńska, C. Semprimoschnig, *Addit. Manuf.* **2018**, *24*, 606.
[15] A. Gladman, E. A. Matsumoto, R. G. Nuzzo, L. Mahadevan, J. A. Lewis, *Nat. Mater.* **2016**, *15*, 413.

[16] H. S. Van, *Compos. Struct.* **2019**, *210*, 869.
[17] C. de Kergariou, F. Demoly, A. Perriman, A. Le Duigou, F. Scarpa, *Adv. Funct. Mater.* **2023**, *33*, 2210353.
[18] V. S. C. Chillara, M. L. Dapino, *Appl. Mech. Rev.* **2020**, *72*, 010801.
[19] Q. Wang, X. Tian, L. Huang, D. Li, A. V. Malakhov, A. N. Polilov, *Mater. Des.* **2018**, *155*, 404.
[20] A. Le Duigou, G. Chabaud, F. Scarpa, M. Castro, *Adv. Funct. Mater.* **2019**, *29*, 201903280.
[21] M. Bodaghi, S. V. Hoa, T. Gries, A. Le Duigou, Y. Tadesse, L. Yao, A. Zolfagharian, *Smart Mater. Struct.* **2023**, *32*, 110401.
[22] C. F. Alban, C. C. Perry, *Mach. Des.* **1959**, *143*.
[23] T. van Manen, S. Janbaz, K. M. B. Jansen, A. A. Zadpoor, *Commun. Mater.* **2021**, *2*, 56.
[24] R. M. Erb, J. S. Sander, R. Grisch, A. R. Studart, *Nat. Commun.* **2013**, *4*, 1712.
[25] A. Le Duigou, M. Grabow, M. Castro, R. Toumi, M. Ueda, R. Matsuzaki, Y. Hirano, J. Dirrenberger, F. Scarpa, R. D'Elia, K. Labstie, U. Lafont, *Heliyon* **2023**, *9*, e13581.
[26] C. Morvan, C. Andème-Onzighi, R. Girault, D. S. Himmelsbach, A. Driouich, D. E. Akin, *Plant Physiol. Biochem.* **2003**, *41*, 935.
[27] P. P. Gillis, R. E. Mark, *Cellulose Chem. Technol.* **1973**, 209.
[28] I. D. Cave, *Wood Sci. Technol.* **1978**, *12*, 75.
[29] I. Burgert, M. Eder, N. Gierlinger, P. Fratzl, *Planta* **2007**, *226*, 981.
[30] N. Plaza, S. L. Zelinka, D. S. Stone, J. E. Jakes, *Smart Mater. Struct.* **2013**, *22*, 072001.
[31] J. E. Jakes, N. Plaza, S. L. Zelinka, D. S. Stone, S. C. Gleber, S. Vogt, *Proc. of SPIE* **2014**, *9055*.
[32] R. E. Mark, J. L. Thorpe, A. J. Angelo, R. W. Perkins, P. P. Gillis, *J. Polym. Sci. Part C* **1971**, *36*, 177.
[33] E. Reyssat, L. Mahadevan, *J. R. Soc. Interface.* **2009**, *6*, 951.
[34] A. Bourmaud, J. Beaugrand, D. U. Shah, V. Placet, C. Baley, *Prog. Mater. Sci.* **2018**, *97*, 347.
[35] V. Placet, O. Cisse, M. L. Boubakar, *J. Mater. Sci.* **2011**, *47*, 3435.
[36] B. M. Finio, R. J. Wood, presented at IEEE/RSJ International Conference on Intelligent Robots and Systems, San Francisco, California, U.S.A, September **2011**.
[37] M. Ashby, *Materials Selection in Mechanical Design*, Butterworth-Heinemann, Oxford **1999**.
[38] S. Coyle, C. Majidi, P. LeDuc, K. J. Hsia, *Extreme. Mech. Lett.* **2018**, *22*, 51.
[39] G. Chabaud, M. Castro, C. Denoual, A. Le Duigou, *Addit. Manuf.* **2019**, *26*, 94.
[40] T. van Manen, S. Janbaz, A. A. Zadpoor, *Mater. Horiz.* **2017**, *4*, 1064.